Parameters calibration and experimentation of a discrete element model for tomato stems

Xifeng Liang
lxfcjlu@163.com
China Jiliang University
Taiyang Wang
China Jiliang University
Wenshuo Gao
China Jiliang University
Hui Zhang
Zhejiang Provincial Agricultural Technology Extension Center
Yebo Qin
Zhejiang Provincial Agricultural Technology Extension Center

Article

Keywords: pruning robot, tomato stems, shear simulation, Box-Behnken, error reduction

Posted Date: May 5th, 2026

DOI: https://doi.org/10.21203/rs.3.rs-9042683/v1

Additional Declarations: No competing interests reported.

Parameters calibration and experimentation of a discrete element model for tomato stems

Xifeng Liang,[1] Taiyang Wang,[1] Wenshuo Gao,[1] Hui Zhang,[2] Yebo Qin[2]

[1]School of Mechanical and Electrical Engineering, China Jiliang University, 310018, Hangzhou, China;

[2]Zhejiang Provincial Agricultural Technology Extension Center , 310018, Hangzhou, China

Corresponding author: Xifeng Liang, School of Mechanical and Electrical Engineering, China Jiliang University, Hangzhou, China. E-mail: lxfcjlu@163.com

Author Contributions: All authors made a substantive intellectual contribution, read and approved the final version of the manuscript and agreed to be accountable for all aspects of the work.

Competing interests: The authors declare no known competing financial interests of this paper.

Funding
This research was supported by the National Natural Science Foundation of China (Grant No. 32372007).

Abstract

The effective optimization of tomato pruning robots was hindered by the lack of accurate simulation models for the shearing process of tomato stems and precise calibration and optimization methods for bonding parameters to predict shearing force. This paper proposed a simulation model along with a bonding parameter calibration method. Taking shearing force as the evaluation metric, a two-level factorial experiment was conducted to screen for significant parameters. A steepest ascent experiment was employed to determine the optimal range of these significant parameters. Then a Box-Behnken design was implemented, and the optimal combination of bonding parameters was derived based on the established regression model. Finally, comparative experiments were conducted to validate the simulation's shearing performance under this optimal parameter set. The results show that the optimal combination for the tomato stem model bonding parameters was a normal stiffness x_3=2.05×10^8 N·m^{-3}, tangential stiffness x_8=1.62×10^8 N·m^{-3}, and a bonding radius x_{21}=3.26×10^{-4} m. The optimized model reduced the shearing force simulation error by 75.8 and 43.7 percentage points compared to the traditional and pre-optimization models. These results demonstrate that the calibrated parameters of the simulation model are accurate and reliable. It can provide valuable parameters for optimizing the design of a tomato pruning robot.

Keywords: pruning robot, tomato stems, shear simulation, Box-Behnken, error reduction.

Introduction

In recent years, the tomato industry has been expanding in scale, having emerged as one of the most important leading agricultural commodities worldwide. Despite its significant economic value and extensive cultivation area, the level of automation in tomato production around the world remains relatively low [1]. Among the various stages of tomato cultivation, the labor costs associated with pruning and harvesting alone account for more than 70% of the total production costs [2].

To address the requirements for automatic pruning, considerable research has been conducted globally on tomato pruning robots. For example, the Dutch company Kompano has developed an automated tomato leaf removal machine capable of managing pruning tasks in a greenhouse covering an area of 2 hectares per day. Other studies have utilized image processing and deep learning techniques to develop visual recognition systems for identifying lateral shoots, thereby improving pruning accuracy [3]. Furthermore, flexible end-effectors have been designed to standardize operations and reduce mechanical damage to plants during pruning [4]. Although significant progress has been made in the development of end-effectors for tomato pruning, the interaction mechanism between these end-effectors and tomato stems remains poorly understood. To reduce experimental costs and enable visual analysis of results, numerical simulation techniques [5] are commonly employed to study interactions between materials and mechanical components. However, existing studies often rely on rigid stem models [6], which fail to simulate key mechanical behaviors of tomato stems during pruning, such as tensile and shear responses. Therefore, to accurately simulate these mechanical processes, it is necessary to develop a breakable Discrete Element Model of the tomato stem.

Meanwhile, researchers around the world have conducted in-depth studies on the construction of discrete element models for plant stems [7]. Measured parameters of spinach roots, analyzed the shovel-cutting process, investigated the working mechanism, optimized the cutting shovel parameters, and ultimately developed a discrete element model. Similarly, other scholars have adopted comparable approaches to construct DEMs for flax stems [8], forage rape stems [9], wheat straw [10], and flexible corn stalks [11]. However, in these DEM modeling methods for stems, crops are typically treated as isotropic materials and simplified into a single tissue structure, resulting in EDEM simulation models composed of bonded particles with uniform properties. When stems exhibit internal multi-layer structures and anisotropic characteristics, the use of uniformly attributed particles in simulations can lead to significant errors.

To address the issue of significant differences in the mechanical properties between the epidermis and pith of bolting rapeseed stems in the clamping section, [12] employed the Hertz-Mindlin with Bonding contact model and utilized two types of particles with distinct material properties to simulate the epidermis and pith, thereby establishing a double-layer bonded discrete element model for bolting rapeseed stems at the harvesting stage. Similarly, [13] developed separate discrete element models for the bark and core of ramie stems, simulated the decortication process, and identified the optimal configuration for the ramie stem separation device. Compared to single-layer stem modeling approaches, such methods yield higher accuracy and better reflect the differences in mechanical properties of the internal stem structures.

When establishing a discrete element model, the required parameters mainly include intrinsic parameters, contact parameters, and bonding parameters. Intrinsic parameters consist of Poisson's ratio, shear modulus, and density; contact parameters include the coefficient of restitution, static friction coefficient, and rolling friction coefficient; bonding parameters mainly comprise normal stiffness, tangential stiffness, critical normal stress, critical tangential stress, and bonding radius. While intrinsic and contact parameters can be directly measured [14,15], bonding parameters are difficult to obtain through direct measurement [16] measured the tensile stiffness and fracture strength of grape bunch stems to establish a discrete element model for grape bunches and calibrated the model parameters via simulation experiments. Although some bonding parameters can be acquired through measurement and calculation, discrete element models are generally simplified representations, making it challenging to maintain complete consistency between the model and reality. Therefore, validation through both simulation and physical testing is essential [17].

This study focuses on tomato stems and addresses their heterogeneous internal mechanical properties by employing the Hertz-Mindlin with Bonding contact model. A three-layer bonded Discrete Element Method model of the tomato stem was developed using three distinct particle sizes for particle filling. The bonding parameters were subsequently calibrated based on the Design of Experiments methodology. The calibrated model was then utilized to simulate the mechanical behavior of tomato stems during a shear process. Simulation results demonstrated close agreement with actual shear tests, validating the model's accuracy. This approach provides a valuable reference for investigating the mechanical characteristics of tomato stems and optimizing the end-effectors of tomato pruning robots.

Materials and Methods

Measurement of Tomato Stem Physical Properties

The tomato stems used in the experiment were obtained from the 'Zheza No.8' cultivar of large-fruited tomato. The study focused on the basal sections of the lateral branches, with the specific sampling location illustrated in Figure 1. The internal structure of the tomato stem can be divided into the cortex, xylem, and pith, as shown in Figure 2. For pruning large tomato plants, the diameter of lateral branches typically ranges from 5 mm to 7.5 mm. Stems with a diameter of approximately 7.5 mm were collected, and their leaves and side shoots were removed. Through repeated measurements and calculations, the following physical property parameters were determined: an average stem length of 50 mm, an average diameter of 7.5 mm, and an average moisture content of 69.5%. To establish an accurate Discrete Element Model of the tomato stem and provide reference values for calibrating the bonding parameters, shear tests were performed on the stems. The shear tests were conducted using an FTC texture analyzer at a loading speed of 2 mm/s. For tomato stems with a diameter of 7.5 mm, five repeated tests were performed to measure the shear force.

Fig.1 Tomato stem sampling position

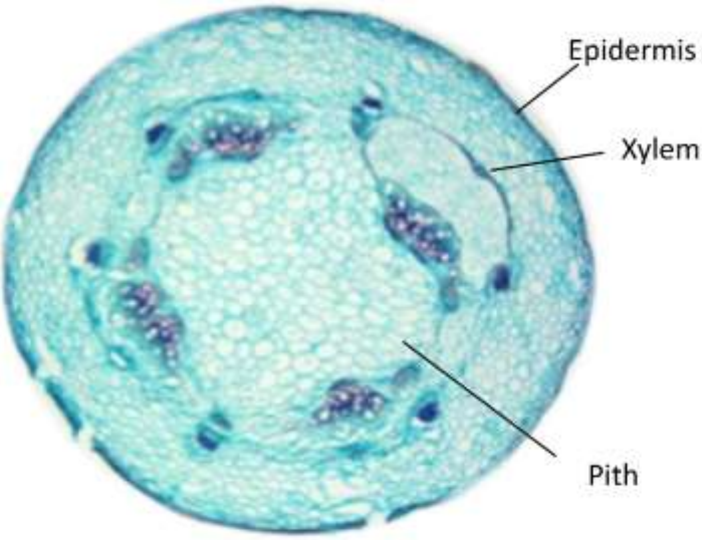

Fig.2 Tomato stem's microscopic tissue structure

Intrinsic and Contact Parameters of the Tomato Stem

To establish the discrete element model, it was necessary to acquire the intrinsic parameters of tomato stems, including density (ρ), Poisson's ratio (μ), and shear modulus (G). These parameters were determined through experimental measurements and by referencing existing research findings.

The average density of the tomato stem samples with a diameter of 7.5 mm was determined to be 960.5 kg/m³. This was calculated by measuring the mass and volume of the samples using an electronic balance and a vernier caliper, respectively. Poisson's ratio has been reported to have an insignificant influence on simulation outcomes [18]. The referred parameter is 0.34, which is adopted in this study based on values reported of similar plant stems [19,20].

The elastic modulus of the tomato stems was measured directly via tensile tests. From this, the shear modulus was calculated. In the tensile tests, the ends of the stem specimens were secured by fixtures and stretched at a speed of 5 mm/s until complete fracture occurred. Five replicate tests were conducted, yielding an average elastic modulus. The shear modulus was subsequently calculated using the following established relationship:

$$G=\frac{E}{(2(1+\mu))} \tag{Eq.1}$$

Where: G, shear modulus (Pa); E, elastic modulus (Pa); μ, Poisson's ratio.

The coefficient of restitution was determined using a 45° inclined plate impact test [21], as shown in Figure 3. In this test, a tomato stem was raised to a height H above the plate and positioned to ensure a radial impact during free fall. Upon release, the stem underwent free fall, collided radially with the inclined plate, rebounded, and subsequently landed on a collection plate, producing a horizontal displacement S_1. The vertical distance between the impact point and the collection plate was recorded as H_1. The procedure was repeated by varying this vertical distance to H_2, and the corresponding horizontal displacement S_2 was measured.

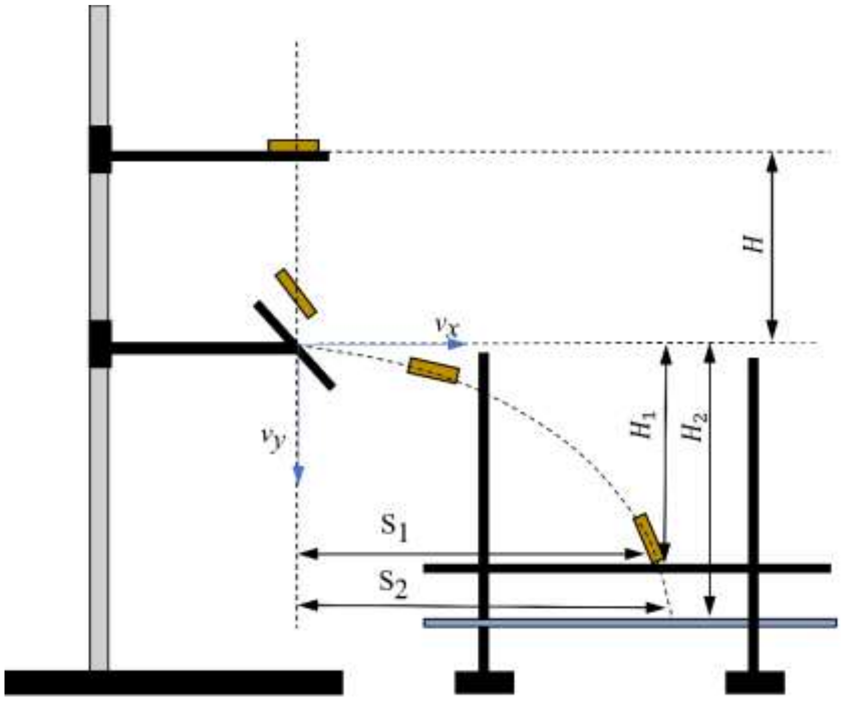

Fig.3 Tomato stem recovery coefficient measurement device schematic diagram

The coefficient of restitution between the sample and the inclined plate was calculated using the following equation [22]:

$$e=\frac{\sqrt{v_x^2+v_y^2}cos\left(45°+arctan\frac{v_y}{v_x}\right)}{v_0 sin45°} \tag{Eq.2}$$

$$\begin{cases} v_x=\sqrt{\frac{gS_1S_2(S_1-S_2)}{2(H_1S_2-H_2S_1)}} \\ v_y=\frac{H_1v_x}{S_1}-\frac{gS_1}{2v_x} \end{cases} \tag{Eq.3}$$

Where: v_0, vertical velocity component before collision (m/s); v_x, horizontal velocity component after collision (m/s); v_y, vertical velocity component after collision (m/s); g, gravitational acceleration (m/s^2).

The test was repeated ten times, and the data were recorded. The average value of the coefficient of restitution was determined from the calculations.

The friction coefficients were measured using a custom-developed friction testing apparatus. This setup enables the direct measurement of the friction angle. The static friction coefficient and the rolling friction coefficient were subsequently calculated. During testing, the tomato stem samples were affixed to the apparatus. To minimize the influence of variations in moisture content, all measurements were completed within a short timeframe. The test was repeated ten times to determine the friction coefficients between tomato stems themselves and between tomato stems and alloy steel.

Contact Model of tomato stem

The discrete element model is composed of spherical particles. A Hertz-Mindlin contact model with bonding was employed to establish the tomato stem model. This modeling approach allows for the formation of bonding bonds between particles, enabling the simulation of the biomechanical properties of plant stems through the formation and breakage of these bonds. A schematic diagram of the bonding bonds between particles is presented in Figure 4.

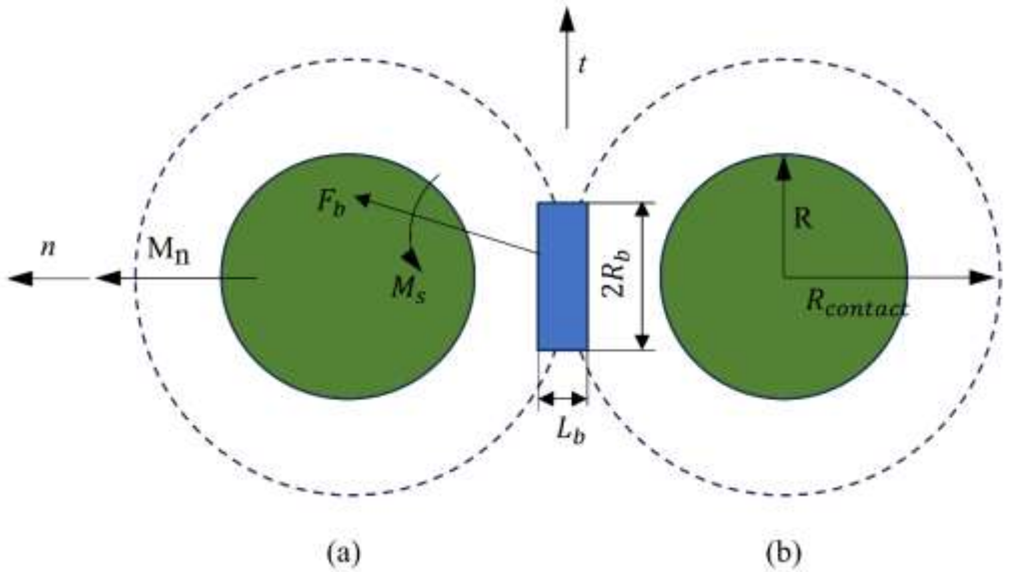

Fig.4 Contact model and its adhesive bonds:(a) Particle A;(b) Particle B

In the diagram, F_b represents the resultant force exerted by Particle A on Particle B; M_n and M_s denote the normal and tangential moments, respectively; n and t are the unit vectors in the normal and tangential directions, respectively; L_b is the overlap between Particle A and Particle B; R_b is the bonding radius; R is the particle radius; and R_{contact} is the contact radius. To ensure sufficient connection between particles, the contact radius R_{contact} is set to be 20% to 30% larger than the particle radius R. The forces and moments acting on a particle are calculated using the following equations:

$$\delta F_n = v_n k_b^n A' \delta_t \tag{Eq.4}$$

$$m\delta F_t = v_t k_b^s A' \delta_t \tag{Eq.5}$$

$$\delta M_n = \omega_n k_b^s J \delta_t \tag{Eq.6}$$

$$\delta M_s = \omega_t k_b^n J \delta_t / 2 \tag{Eq.7}$$

where:A', contact area (mm^2); $k_b{}^n$, normal stiffness per unit area (N/m^3); $k_b{}^s$, shear stiffness per unit area (N/m^3); δ_t, time step (s); v_n,v_t, normal and tangential velocities (m/s); ω_n,ω_t, normal and tangential angular velocities (rad/s); δM_n,δM_s, incremental normal and tangential moments (N·m); δF_n,δF_t, incremental normal and tangential cohesive forces (N); J, moment of inertia (mm^4).

The tangential and normal forces between particles act on the bonding bond. Due to particle motion (translation or rotation), the bond fractures when the stress exceeds a predefined threshold, according to the following criteria:

$$\sigma_{max} < \frac{-F_n}{A'} + \frac{2M_t}{J} R_b \tag{Eq.8}$$

$$\tau_{max} < \frac{-F_t}{A} + \frac{2M_n}{J} R_b \quad \text{(Eq.9)}$$

where: σ_{max}, critical normal stress (Pa); τ_{max}, critical shear stress (Pa); R_b, bonding radius (m).

Tomato Stem Model Construction

Observation of the tomato stem's internal microstructure reveals that the epidermis constitutes a small proportion of the cross-section and possesses low structural strength; the xylem accounts for a larger share and exhibits high structural strength; while the pith, although the most voluminous component, is heterogeneous and composed of soft, porous tissue. To streamline the discrete element model and enhance computational efficiency, one approach is to scale up the internal structural dimensions and represent them with identical particles, albeit at the cost of reduced model accuracy. Alternatively, filling the stem model with distinct particle types yields biomechanical characteristics that more closely align with those of actual plant stems. Consequently, the discrete element model developed in this study represents the 7.5 mm diameter tomato stem by separately modeling the epidermis, xylem, and pith using particles of different sizes: 1.0 mm, 0.375 mm, and 0.5 mm in diameter, respectively. The resulting tomato stem discrete element model comprises 18,018 particles and generates 79,286 bonding bonds, to evaluate the effect of the bond enhancement, a traditional model was constructed in parallel to serve as a baseline for comparison, as shown in Figure 5.

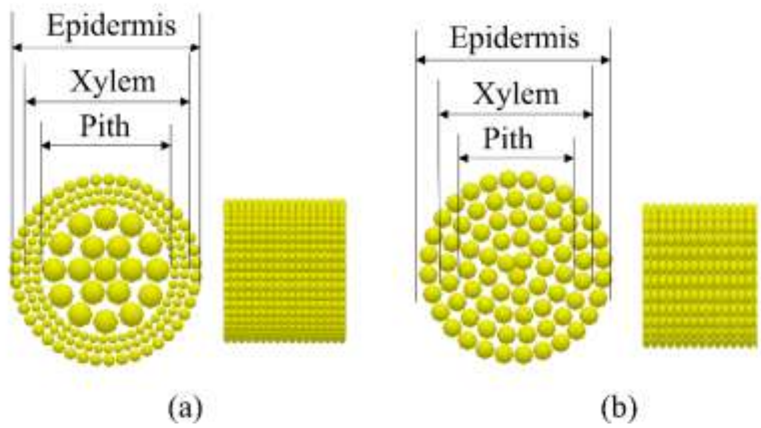

Fig.5 Discrete element model of tomato stems:(a) Enhanced tomato stem model; (b) Traditional tomato stem model

Bonding Parameter Calibration with Initial Values

A shear simulation test of tomato stems was conducted with shear force as the target response. A two-level factorial design was first employed to screen for factors exerting significant effects on the shear force. This was followed by a steepest ascent experiment to determine the optimal region of these significant factors. Finally, response surface methodology was applied to establish a regression model for the significant factors, leading to the identification of the optimal parameter combination.

The key parameters governing the bonding bonds between particles in the Hertz-Mindlin with Bonding contact model include the normal stiffness Kn, tangential stiffness Ks, critical normal stress σ, critical tangential stress τ, and bonding radius Rj [23,24]. These parameters are governed by the following equations:

$$\begin{cases} K_n=\frac{4}{3}\left(\frac{1-\varepsilon_a^2}{E_a}+\frac{1-\varepsilon_b^2}{E_b}\right)^{-1}\left(\frac{r_a+r_b}{r_ar_b}\right)^{-\frac{1}{2}} \\ K_s=\left(\frac{1}{2}\sim\frac{2}{3}\right)K_n \\ \sigma=\frac{F}{\pi R^2} \\ \tau=c+\sigma tan\varphi \end{cases} \tag{Eq.10}$$

Where: ε_a,ε_b, Poisson's ratio of particles; E_a,E_b, Elastic modulus of particles (MPa); r_a,r_b, Particle radius (mm); R, Radius of the compression surface (mm); c, Cohesion of the stem material (MPa); φ, Internal friction angle (degree).

The bonding parameters were preliminarily estimated through theoretical calculation. These parameters were designated as the experimental factors x_1 to x_{20} for a two-level factorial design, as listed in Table 1. The bonding radius R_j was additionally set as factor x_{21}=3.25×10^{-4} m. The calculated values for all factors were coded from X_1 to X_{21} and maintained at their center points. A high level and a low level were then assigned to each factor, corresponding to an increase and a decrease of approximately 20% from its central value, respectively.

Table 1 Factors of two-level factorial experiment

	Pith- Pith	Pith -Xylem	Xylem - Xylem	Xylem-Epidermis	Epidermis-Epidermis
K_n/N·m^{-3}	x_1=3.4×10^7	x_2=4.2×10^7	x_3=2×10^8	x_4=8.4×10^7	x_5=6.4×10^7
K_s/N·m^{-3}	x_6=2.3×10^7	x_7=2.8×10^7	x_8=1.3×10^8	x_9=5.6×10^7	x_{10}=4.3×10^7
σ/Pa	x_{11}=3.6×10^6	x_{12}=4×10^7	x_{13}=4×10^7	x_{14}=8.4×10^6	x_{15}=8.4×10^6
τ/Pa	x_{16}=1.2×10^7	x_{17}=3.2×10^7	x_{18}=3.2×10^7	x_{19}=1.6×10^7	x_{20}=1.6×10^7

Two-Level Factorial Design and Steepest Ascent Test

The coded factors X_1 to X_{21} were assigned high and low levels for the two-level factorial experiment. With the shear force of the tomato stem set as the target response for the simulation, a two-level factorial design comprising 32 simulation trials was constructed. This design effectively screened for the parameters exerting the most significant influence on the shearing force.

Based on the results of the factorial experiment, the parameters identified as having a significant effect on shear force were selected for a subsequent steepest ascent test.

All non-significant factors were fixed at their central level. Six trial points were arranged along the path of steepest ascent. As the levels of the significant factors were systematically adjusted, the simulated shear force changed accordingly. The trial point yielding a shear force closest to the experimentally measured value was identified. The factor levels from this point and its adjacent predecessor were then designated as the low and high levels, respectively, for the subsequent Box-Behnken design.

Box-Behnken Experiment

To obtain the optimal combination of bonding parameters, with shear force as the response variable, a three-factor, three-level Box-Behnken response surface design was conducted using Design-Expert software, based on the results from the previous two-level factorial and steepest ascent tests [25,26]. The results of the response surface experiments were analyzed and fitted to establish a second-order regression model describing the relationship between shear force and the influencing factors. A comprehensive analysis of the Box-Behnken response surface results was subsequently performed.

Results

Experimental Results of Stem Model Parameter Testing

Shear tests were performed on tomato stems with a diameter of 7.5 mm. Five replicate tests yielded an average shearing force of 28.9 N. The results of the intrinsic parameter tests were as follows: density $\rho = 960.5\ \mathrm{kg \cdot m^{-3}}$, Poisson's ratio $\mu = 0.34$, and shear modulus $G = 3.4 \times 10^7$ Pa. The results of the contact parameter tests are summarized in Table 2.

Table 2 Tomato stem contact parameters

Contact Materials	Parameter	Mean Value
Tomato Stem – Tomato Stem	Coefficient of Restitution	0.41
	Static Friction Coefficient	0.56
	Rolling Friction Coefficient	0.24
Tomato Stem – Alloy Steel	Coefficient of Restitution	0.51
	Static Friction Coefficient	0.62
	Rolling Friction Coefficient	0.28

Results of the Two-Level Factorial and Steepest Ascent Tests

The analysis of variance for the two-level factorial design identified factors with P-values less than 0.01, as summarized in Table 3. As shown in the table, the model's P-value is far below 0.05, indicating that the results are statistically significant.

Specifically, the coded factors X_3 (normal stiffness of xylem-xylem contact), X_8 (tangential stiffness of xylem-xylem contact), and X_{21} (particle bonding radius) all have P-values less than 0.01. This demonstrates that the corresponding parameters—xylem-xylem normal stiffness (x_3), xylem-xylem tangential stiffness (x_8), and particle bonding radius (x_{21})—exert a significant influence on the shear force. In contrast, the effects of the remaining factors were negligible.

Table 3 ANOVA for Two-Level Factorial Experiments

Source of Variation	F/N				
	Mean square	Df	Sum of squares	F value	P value
Model	10.116	21	212.429	27.920	$< 0.001^{**}$
X_3	191.590	1	191.590	528.799	$< 0.001^{**}$
X_8	7.315	1	7.315	20.191	$<0.001^{**}$
X_{21}	9.790	1	9.790	27.022	$< 0.001^{**}$

Based on the results of the two-level factorial design, the parameters that exhibited a significant influence on the shear force of the tomato stem—namely X_3, X_8, and X_{21}—were selected for the steepest ascent test. All non-significant factors were held constant at their central level. The experimental design and results are presented in Table 4. As the levels of these factors increased incrementally along the steepest ascent path, the simulated shear force of the tomato stem gradually increased. Specifically, the shear forces recorded for Trial 1 and Trial 3 were 27.4 N and 32.3 N, respectively. The factor levels corresponding to Trial 1 and Trial 3 were subsequently designated as the low and high levels for the ensuing Box-Behnken experimental design.

Table 4 Scheme and results of steepest ascent test

No.	Factor			F/N
	$x_3/(N \cdot m^{-3})$	$x_8/(N \cdot m^{-3})$	x_{21}/m	
1	2×10^8	1.3×10^8	3.25×10^{-4}	27.4
2	2.4×10^8	1.56×10^8	3.30×10^{-4}	29.8
3	2.8×10^8	1.82×10^8	3.35×10^{-4}	32.3
4	3.2×10^8	2.08×10^8	3.40×10^{-4}	33.9
5	3.6×10^8	2.34×10^8	3.45×10^{-4}	36.2
6	4×10^8	2.6×10^8	3.50×10^{-4}	38.5

Results of the Box-Behnken Experiment

To obtain the optimal combination of bonding parameters, the experimental design and corresponding results are presented in Table 5. Based on the analysis and fitting of the Box-Behnken experiment results, a second-order regression model describing the relationship between shear force and the influencing factors was established as follows:

$F = 29.8 + 1.9X_3 + 0.0625X_8 + 0.2875X_{21} - 0.125X_3X_8 + 0.025X_3X_{21} + 0.4X_8X_{21} + 0.4X_3^2 - 0.125X_8^2 - 0.175X_{21}^2$ (Eq.11)

Where: X_3, normal stiffness of xylem-xylem contact coded factor; X_8, tangential stiffness of xylem-xylem contact coded factor; X_{21}, particle bonding radius coded factor.

Table 5 Box-Behnken Experimental Design and Results

number	X_3	X_8	X_{21}	F/N
1	-1	-1	0	28.2
2	0	0	0	29.8
3	0	-1	-1	29.3
4	1	-1	0	32.3
5	1	0	-1	31.6
6	1	1	0	31.7
7	-1	0	-1	27.9
8	0	-1	1	30.7
9	0	0	0	29.8
10	1	0	1	32.2
11	-1	1	0	28.1
12	0	0	0	29.8
13	0	1	-1	29.1
14	-1	0	1	28.4
15	0	1	1	30.5

An analysis of variance was performed on the Box-Behnken design, and the results are presented in Table 6. As shown in Table 6, the second-order regression model has a coefficient of determination (R^2) of 0.986, indicating an excellent fit. The model itself is statistically significant, while the lack-of-fit term is not significant. This suggests that the model adequately captures the relationship within the experimental domain and that no other major factors unaccounted for significantly influence the response value. The factor X_3 has a P-value of less than 0.01, denoting a highly significant effect on the shear force. Furthermore, X_{21}, the interaction term X_8X_{21}, and the quadratic term X_3^2 all have P-values less than 0.05, indicating a significant influence. The effects of the remaining terms are not statistically significant. Response surface plots illustrating the interactive effects of these significant factors on the shearing force are presented in Figure 6.

Table 6 ANOVA for Box-Behnken results

Source of Variation	F/N			
	MS	DF	*F*	*P*
Model	31.104	9	52.88	0.0001**
X_3	28.88	1	441.879	0.0001**
X_8	0.031	1	0.478	0.511

X_{21}	0.661	1	10.117	0.015*
X_3X_8	0.062	1	0.956	0.36
X_3X_{21}	0.002	1	0.038	0.85
X_8X_{21}	0.64	1	9.792	0.016*
X_3^2	0.673	1	10.307	0.014*
X_8^2	0.065	1	1.006	0.349
X_{21}^2	0.128	1	1.972	0.202
Residual	0.457	7		
Lack of Fit	0.457	3		
Pure Error	0	4		
$R^2 = 0.986$				

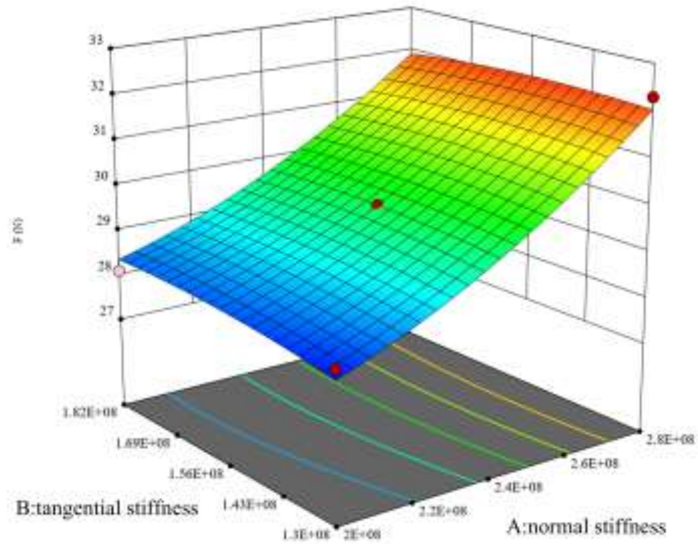

(a)

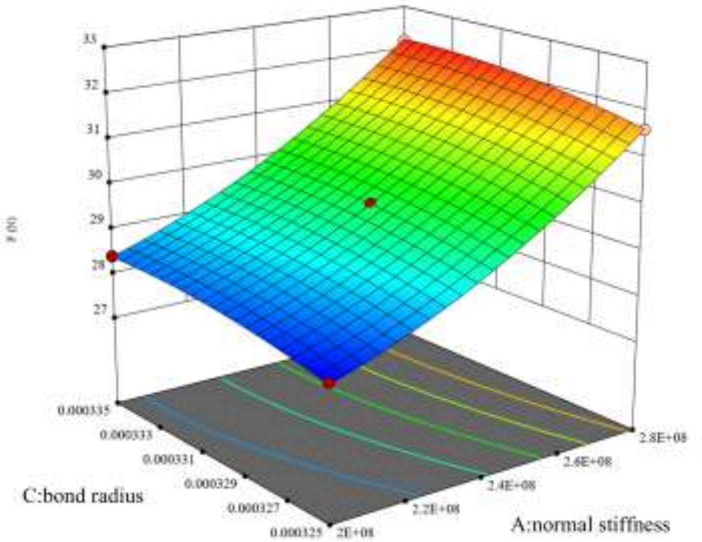

(b)

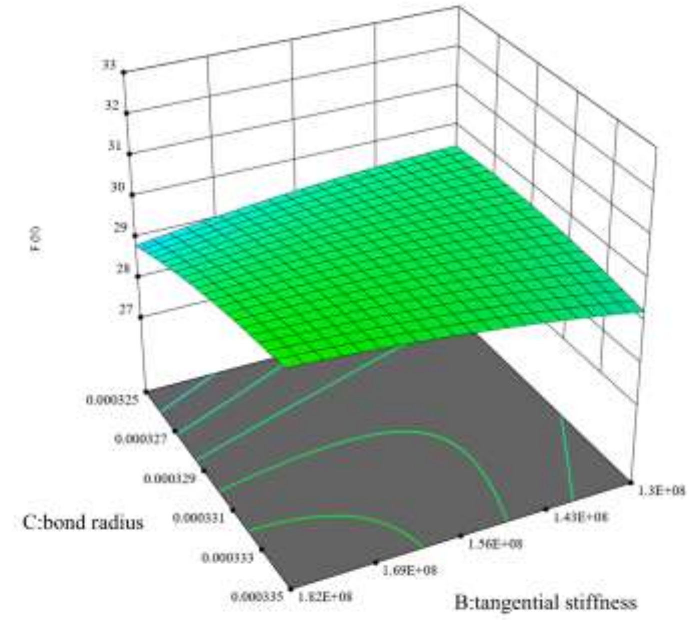

(c)

Fig.6 Effect of experimental parameters on shearing force:(a) Effect of normal stiffness and tangential stiffness; (b) Effect of normal stiffness and bond radius; (c) Effect of tangential stiffness and bond radius

As shown in Figure 6, when the bonding radius x_{21} was fixed at 3.30×10^{-4} m, the shearing force reached its minimum value of 28.1 N at a normal stiffness x_3 of 2×10^8 $N\cdot m^{-3}$ and a tangential stiffness x_8 of $1.82\times10^8 N\cdot m^{-3}$. The shear force increased with increasing normal stiffness x_3 and decreasing tangential stiffness x_8, reaching its maximum value of 32.3N when x_3 was $2.8\times10^8 N\cdot m^{-3}$ and x_8 was $1.3\times10^8 N\cdot m^{-3}$ .With the tangential stiffness x_8 fixed at $1.56\times10^8 N\cdot m^{-3}$, the shearing force exhibited a minimum of 27.9N at a normal stiffness x_3 of $2.8\times10^8 N\cdot m^{-3}$ and a bonding radius x_{21} of 3.25×10^{-4} m. The shear force increased with simultaneous increases in both normal stiffness x_3 and bonding radius x_{21}, achieving a maximum of 32.2 N when x_3 was $2.8\times10^8 N\cdot m^{-3}$ and x_{21} was 3.35×10^{-4} m. When the normal stiffness x_3 was held constant at $2.4\times10^8 N\cdot m^{-3}$, the shear force increased with concurrent increases in both tangential stiffness x_8 and bonding radius x_{21}. The maximum shear force under this condition was 30.5 N, observed at and x_{21}=3.35×10^{-4} m.

Optimal Parameter Combination and Validation

Using the actual shear force of the tomato stem as the target response, the fitted regression equation was solved to obtain the optimal combination of the statistically significant parameters: normal stiffness x_3=2.05×10^8 $N\cdot m^{-3}$, tangential stiffness x_8=1.62×10^8 $N\cdot m^{-3}$, and bonding radius x_{21}=3.26×10^{-4} m. All remaining parameters were maintained at their central levels. A simulated shear test was conducted in EDEM using this optimal parameter set. For comparison, parallel simulations were performed using both a traditional tomato stem model and the pre-optimized model.

The simulated shearing process of the discrete element model alongside the physical shear test is illustrated in Figure 7. A comparison of the force-time curves obtained from the simulation and the physical experiment is presented in Figure 8. The force values and times for these peaks are compared in Figure 9. As shown in Figure 9, the first peak force and time were: 20.8 N and 2.63 s for the physical test; 13.3 N and 1.68 s for the traditional model; 18.8 N and 2.88 s for the pre-optimized model; and 17.6 N and 2.77 s for the optimized model. The second peak force and time were: 28.9 N and 3.93 s for the physical test; 25.2 N and 3.79 s for the traditional model; 30.5 N and 4.03 s for the pre-optimized model; and 29.8 N and 3.99 s for the optimized model.

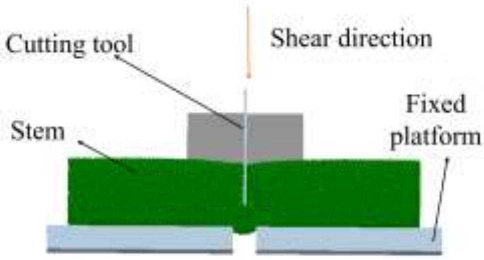

(a)

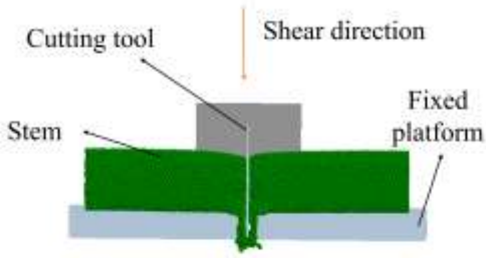

(b)

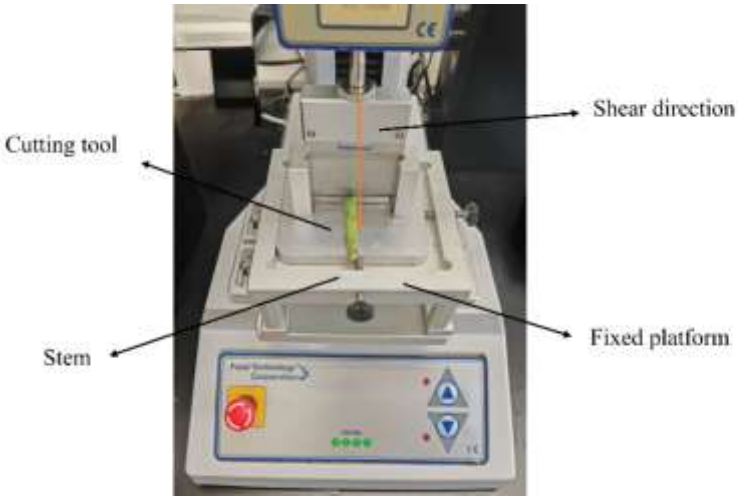

(c)

Fig.7 Simulation and physical shearing tests of tomato stem:(a) Stem model shearing; (b) Stem model fracture; (c) Physical shearing.

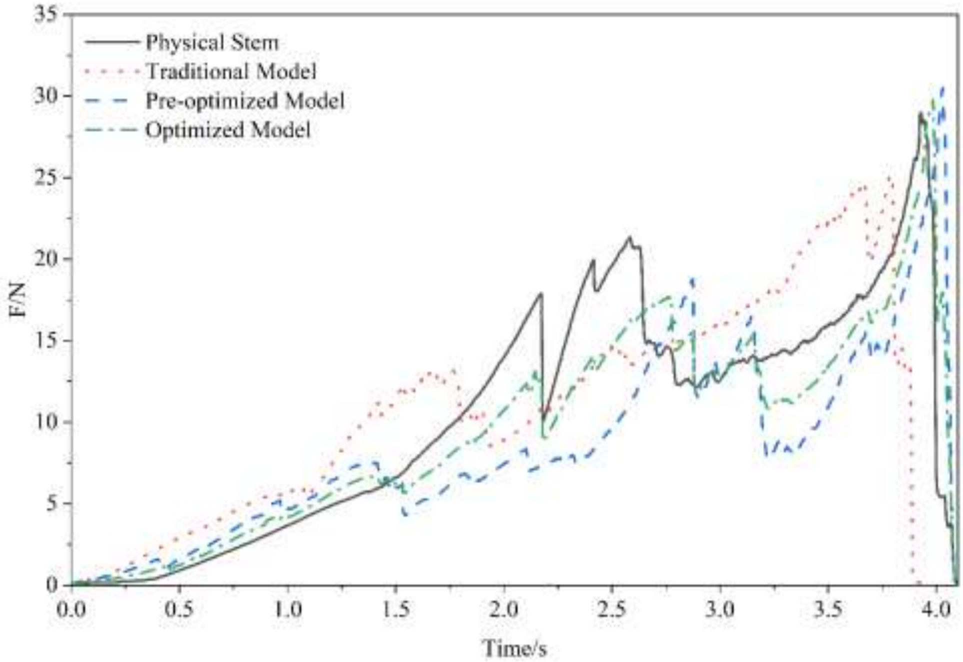

Fig.8 Shear force-time curve of tomato stems

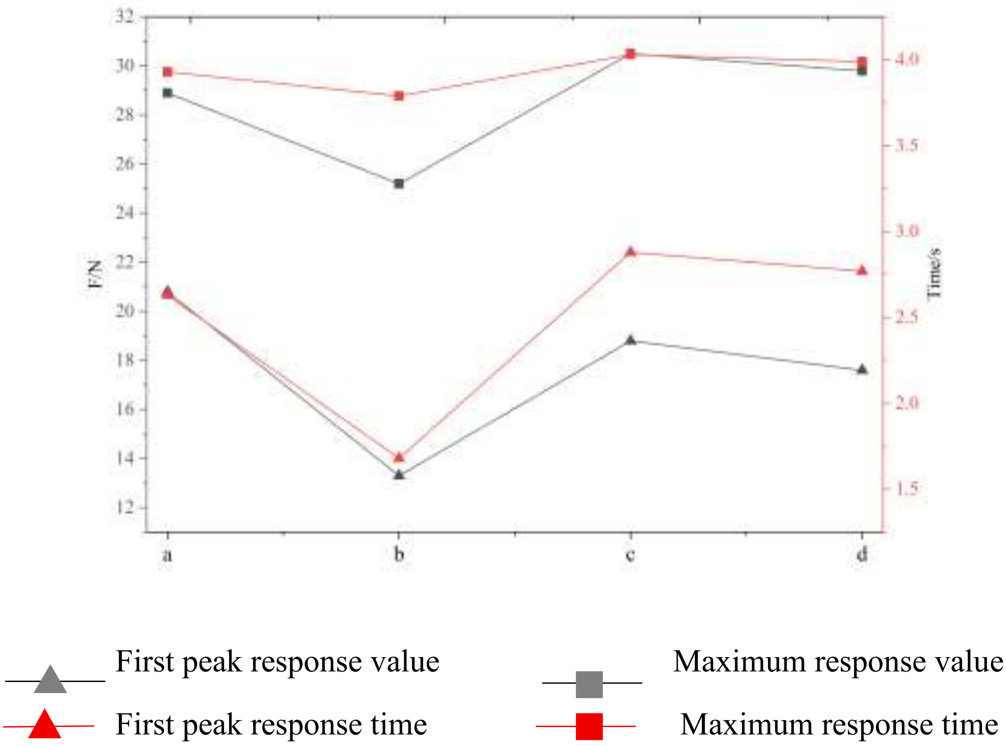

Fig.9 Peak response value and time of shearing tests

The traditional model exhibited substantial errors in both response magnitude and response speed at the two shear force peaks compared to the physical tomato stem.

The pre-optimized model also showed considerable error in the response speed and the maximum peak response value at the first peak. In contrast, the optimized model demonstrated significant improvement: it reduced the error in response speed at the first peak by 85.3% and 44.2% relative to the traditional and pre-optimized models, respectively. Furthermore, the errors in the maximum peak response value and the corresponding response speed were reduced by 75.8%, 43.7%, 58.3%, and 40%, respectively, compared to the two baseline models. These results indicate that the tomato stem model with the optimal parameter set achieves highly accurate simulation performance, confirming that the calibrated and optimized parameters are both reliable and effective.

Conclusions

This study proposed a tomato stem model along with a method for calibrating and optimizing its bonding parameters. The physical properties of the stem were determined through experimental measurements. To obtain ideal values for the bonding parameters, calibration and optimization were performed via a series of tests, and the applicability of the model under the optimal parameters was verified. Comparative experiments were finally conducted to validate the accuracy of the optimized model. The following conclusions were drawn from this investigation:

(a) For a 7.5 mm diameter tomato stem, the measured physical properties were: density = 960.5 kg/m^3, Poisson's ratio = 0.34, shear modulus = 3.4×10^7 Pa, and shearing force = 28.9 N.

(b) After establishing the tomato stem model, a two-level factorial design was first used to screen for factors significantly affecting shear force. A steepest ascent test was then applied to narrow the calibration range of these significant parameters. Subsequently, a Box−Behnken design was employed to develop a mathematical regression model between the target response (shear force) and three test factors: xylem–xylem normal stiffness, xylem–xylem tangential stiffness, and bond radius. Analysis of variance revealed the influence and interactions of these factors on shear force. The optimal parameter combination was determined as follows: normal stiffness $x_3 = 2.05\times10^8$ $N{\cdot}m^{-3}$, tangential stiffness $x_8 = 1.62\times10^8$ $N{\cdot}m^{-3}$, and bond radius $x_{21} = 3.26\times10^{-4}$ m.

(c) In comparative shear tests, the measured shear forces for the physical stem, the traditional model, the pre-optimized model, and the optimized model were 28.9 N, 25.2 N, 30.5 N, and 29.8 N, respectively. The results show that the optimized model reduces the error in shear force by 75.8% and 43.7% compared to the traditional and pre-optimized models, demonstrating high simulation accuracy and confirming the reliability of the optimal parameter set.

Data availability: All data in this study can be available access from the corresponding author.

References

1. O. Idama & H. Uguru. Robotization of Tomato Fruits Production to Enhance Food Security. *Journal of Engineering Research and Reports,* 67-75 (2021).
2. Elisa A ,Ivan P ,Giuseppina P , et al. Winter Greenhouse Tomato Cultivation: Matching Leaf Pruning and Supplementary Lighting for Improved Yield and Precocity. *Agronomy,* 13 (3), 671-671 (2023).
3. Feng, Q.C., et al. Method for identifying tomato plants pruning point using Mask R-CNN. *Transactions of the Chinese Society of Agricultural Engineering.* 38(3), 128-135 (2022).
4. Wang, B.W., Zhang, W.H., Feng, Q.C. Design and experiment of cutting type tomato pruning operation actuator. *J. Agric. Mech. Res.* 46(10), 53-9+65 (2024).
5. Zeng, Z.W., Ma, X., Cao, X.L. Critical review of applications of discrete element method in agricultural engineering. *Transactions of the Chinese Society for Agricultural Machinery.* 52(4), 1-20 (2021).
6. Wang, B.W., Zhang, W.H., Feng, Q.C. Measurement and analysis of mechanical properties of stem clamping for automatic pruning of tomato. *J. Agric. Mech. Res.*45(12), 157-163 (2023).
7. Yuan, J., Li, J.G., Zou, L.L. Optimal design of spinach root-cutting shovel based on discrete element method. *Transactions of the Chinese Society for Agricultural Machinery.* 51(S2), 85-98 (2020).
8. Shi, R.J., Dai, F., Zhao, W.Y. Establishment of discrete element flexible model and verification of contact parameters of flax stem. *Transactions of the Chinese Society for Agricultural Machinery.*53(10), 146-155 (2022).
9. Liao, Y.T., Liao, Q.X., Zhou, Y. Parameters calibration of discrete element model of fodder rape crop harvest in bolting stage. *Transactions of the Chinese Society for Agricultural Machinery.* 51(6), 73-82 (2020).
10. Matthew, S., Mehari, T. Wheat straw direct shear simulation using discrete element method of fibrous bonded model. *Biosyst. Eng.* 213, 1-12 (2022).
11. Liu, W.H., Su, Q., Fang, M. 2023.Parameters Calibration of Discrete Element Model for Corn Straw Cutting Based on Hertz-Mindlin with Bonding. *Appl. Sci.* 13(2), 1156 (2023).
12. Xie, W., Peng, L., Jiang, P. Discrete element model building and optimization of double-layer bonding of rape shoots stems at harvest stage. *Transactions of the Chinese Society for Agricultural Machinery.* 54(5), 112-120 (2023).
13. Zou, S.C., Su, G.B., Shao, Y.G. Simulation optimization and experiment of separation device for ramie stalks based on discrete element method. *J. Chin. Agric. Mech.*38(1), 60-67 (2017).
14. Han, D.D., Wang, Q., Tang, C. Calibration of the contact parameters for soybean bonded particle model based on discrete element method. *J Mech Sci Technol.* (prepublish): 1-9 (2025).

15. Li, D.D., Wang, R.Y., Zhu, Y.P. Calibration of Simulation Parameters for Fresh Tea Leaves Based on the Discrete Element Method. *Agriculture*. 14(1), 148(2024).
16. Coetzee, C., Lombard, S. The destemming of grapes: Experiments and discrete element modelling. *Biosyst. Eng.* 114(3), 232-248 (2013).
17. Coetzee, C. Calibration of the discrete element method: Strategies for spherical and non-spherical particles. *Powder Technol.* 364(prepublish), 851-878 (2020).
18. Wang, Y., Zhang, Y.T., Yang, Y. Discrete element modelling of citrus fruit stalks and its verification. *Biosyst. Eng.* 200, 400-414 (2020).
19. Zhao, W.S., Chen, M.J., Xie, J.H. Discrete element modeling and physical experiment research on the biomechanical properties of cotton stalk. *Comput. Electron. Agric.*204 (2023).
20. Shi, Y.Y., Jiang, Y., Wang, X.C. A mechanical model of single wheat straw with failure characteristics based on discrete element method. *Biosyst. Eng.* 230, 1-15 (2023).
21. Chen, T., Yi, S.J., Li, Y.F. Establishment of discrete element model and parameter calibration of alfalfa stem in budding stage. *Transactions of the Chinese Society for Agricultural Machinery.* 54(5), 91-100 (2023).
22. Du, Z., Li, D.H., Li X.P. Calibration and experiment of discrete element model parameters for tea stem. *Transactions of the Chinese Society for Agricultural Machinery.* 56(1), 311-320 (2025).
23. Han, D.D., Zhou, Y., Nie, J.S. DEM model acquisition of the corn ear with bonded particle model and its simulated parameters calibration. *Granular Matter.* 26(2) (2024).
24. Zhang, S.L., Zhao, H.B., Wang, X.Z. Discrete element modeling and shear properties of the maize stubble-soil complex. *Comput. Electron. Agric.*204 (2023).
25. Wang, Z.P., Zhu, T., Wang, Y.Z. Simulation and analysis of soil homogenization drills based on discrete element method and response surface methodology. *Particuology.* 88, 128-148 (2024).
26. Tai, Z.K., Tong, X., Xu, H.L. Calibration and Verification of Coated Caragana korshinskii Seeds Based on Discrete Element Method. *Coatings.* 15(4), 387 (2025).